Chemical Engineering Journal 166 (2011) 324–331

Contents lists available at ScienceDirect

Chemical Engineering Journal

journal homepage: www.elsevier.com/locate/cej

DEM-CFD simulations of fixed bed reactors with small tube to particle diameter ratios

T. Eppinger*, K. Seidler, M. Kraume

Chemical and Process Engineering, Technische Universität Berlin, Straße des 17. Juni 135, 10623 Berlin, Germany

ARTICLE INFO

Article history:
Received 19 March 2010
Received in revised form 12 October 2010
Accepted 18 October 2010

Keywords:
DEM
CFD
Fixed bed reactors
Lab-scale

ABSTRACT

A new meshing method for fixed beds consisting of monodisperse spherical particles is presented. The particles are flattened near the particle–particle and particle–wall contact points, respectively, to avoid bad cell qualities. Compared to known methods from literature the modifications are so small that a subsequent correction of these modifications is not necessary. CFD simulations are performed for tube to particle diameter ratios of $3 \leq D/d \leq 10$ in the laminar, transitional and turbulent flow regime and are compared with results from literature concerning porosity and pressure drop. The flow pattern within the bed is also investigated. The random fixed bed is generated with a DEM-code and the fluid domain is meshed with the commercial CFD code STAR-CCM+. The focus of this work is to verify, that physically correct results as well as meshes with a low number of cells and therewith short calculation time can be obtained with this new meshing method.

1. Introduction

Fixed bed reactors are widely used in the chemical and process industry amongst others for catalytic surface reactions. The design of such reactors is often done with simplifications, e.g. with the assumption of plug flow and an equally distributed porosity over the whole fixed bed. These assumptions are not valid for reactors with a small tube to particle diameter ratio which are used for highly exothermal reactions and which are dominated by wall effects. These wall effects constrain the heat transfer from the reaction zone which could lead to a bad reactor performance, catalyst sintering or safety issues. Also a reliable scale-up from lab-scale to full-scale apparatuses could be critical. Furthermore an exact description of the flow, temperature and species field is very important for the simulations of chemical reactions.

Several authors have replaced the constant axial velocity by a velocity, which varies in radial direction, either in an exponential way (Kalthoff and Vortmeyer [1], Winter and Vortmeyer [2]) or according to the radial porosity distribution (Daszkowski and Eigenberger [3], Bey and Eigenberger [4], Giese et al. [5]). In all cases the simulation of the experimental results was more accurate, although this velocity profile does not describe the velocity distribution inside the packed bed very exactly, e.g. regions with stagnant or back flow are neglected.

The experimental setup for determining the velocity profile can be subdivided based on the location of the measurement: amongst others Bey and Eigenberger [4] measured the radial velocity at a cross-section behind the exit of the packing. These measurements may be criticized because the flow profile is strongly influenced by the last one or two particle layer and is deformed by radial circumferential flow components (Drahos et al. [6]). To preserve the flow distribution, Bey and Eigenberger [4] used a monolith at the exit of the packing.

Giese et al. [5] measured the velocity profile within the packed bed with the use of Laser-Doppler-velocimetry. Within one cross-section they obtained around 5000 samples inside and outside the particles. These values are averaged in circumferential direction. The so-called artificial velocity is obtained by averaging the velocities at a fixed radius r if the zero velocities inside the particles are included. If the zero velocities are excluded the interstitial velocity is obtained.

With the increase of computational power in the last years it is possible to use CFD for simulating spatially resolved fixed bed reactors. For such a CFD simulation a 3D structure of the fixed bed is needed and this structure has to be subdivided in small control volumes, this means it has to be meshed. For generating a random packing, the discrete element method (DEM) which was first described by Cundall and Strack [7] can be used.

A crucial point for the mesh generation is the cell quality near the particle–particle and particle–wall contact points, respectively. These cells are either highly skewed, which could lead to convergence problems during the calculation, or the mesh is highly refined in this area, which increases the number of cells and as a direct

* Corresponding author. Tel.: +49 30 314 28733; fax: +49 30 314 21134.
E-mail address: thomas.eppinger@tu-berlin.de (T. Eppinger).

1385-8947/$ – see front matter © 2010 Elsevier B.V. All rights reserved.
doi:10.1016/j.cej.2010.10.053

Nomenclature

d	particle diameter [m]
h	height [m]
r	radial coordinate [m]
v_0	superficial/inlet velocity [m/s]
w_z	axial velocity component [m/s]
z	normalized wall distance
A	area [m^2]
D	tube diameter [m]
L	bed length [m]
R	tube radius [m]
Re_P	particle Reynolds number
V	volume [m^3]

Greek letter

ε	porosity
η	kinematic viscosity [m^2/s]
ρ	density [kg/m^3]

Subscript

b	bed

consequence the computational time. Several methods are presented in literature to avoid this.

In the work by Bai et al. [8] and Atmakidis and Kenig [9] the particles are shrunken by a certain amount, the contact points disappear and cells can be generated between the particles. The shrinking of the particles reduces the solid fraction and therefore the porosity. In a subsequent step porosity and pressure drop must be corrected.

Guardo et al. [10] have suggested to increase the size of the particles by a certain value. Contact points become contact lines or areas, respectively, and the skewness of the cells in this zone is reduced. This method needs also a subsequent correction of the values for porosity and pressure drop.

Ookawara et al. [11] have presented a method where the particles are bridged with small cylinders if the distance between the particles falls below a predefined value. This method also avoids highly skewed cells or a massive number of cells and it could be shown that macroscopic flow properties like the pressure drop are not influenced by this. No information is provided concerning the influence on porosity.

In this work the commercial CFD tool STAR-CCM+ by CD-adapco is used for meshing. The problem described above is avoided by flattening the particles locally in the proximity of the contact points if the distance between two particle surfaces falls below a predefined value. This leads to a small gap between the particles which can be filled with cells of good quality. It is shown that the results achieved by this approach are in good agreement with literature in respect to radial and global porosity and pressure drop. There is no need for any subsequent correction. Moreover, the whole process consisting of packing generation, meshing and calculation is completely automated and optimized and results can be obtained in a short time.

2. Methods

2.1. DEM

The generation of the random packings is carried out with the implemented DEM in the commercial CFD package STAR-CD 4.08 by CD-adapco. Spherical monodisperse particles are initialized randomly within the tubular fluid domain and fall because of gravity to the bottom of the tube. For each of these particles a force balance is formulated and solved which takes into account the gravity force and the interaction between particles and between particles and the tube wall. The DEM simulation stops when a steady state is reached. Steady state means that the velocity of each particle is virtually zero.

Table 1
Used parameters for the DEM simulation.

	Symbol	Value
Particle diameter	d [m]	0.001
Tube diameter	D [m]	0.003–0.010
Particle density	ρ [kg/m^3]	2300
Restitution coefficient	E	0.94
Static friction coefficient	μ_S	10^{-5} to 0.2
Rolling friction coefficient	μ_R	1/100 of μ_S

Table 2
Parameters used for the surface and volume mesh generation.

Base size (= sphere diameter)	0.001 m
Triangle edge size for the surface of spheres	4–10% of base size
Surface grow rate	1.3
Number of boundary layers	2
Thickness of the boundary layers	3% of base size
Minimum distance between two surfaces	12% of corresponding triangle edge length

The resulting porosity of the packed bed depends on the surface roughness [12], the manner of packing [12] and the tube to particle diameter ratio D/d [13]. An overview can be found in [14].

For the DEM simulation parameters are set according to Table 1. Density and restitution coefficient correspond to the values of glass spheres. Static friction and rolling friction depend on the surface roughness of the particles and have to be measured. The values used are typical for catalytic active particles taken from [11].

To validate the DEM simulations the global bed porosity and the radial porosity distribution are compared with literature. To obtain the radial porosity distribution cylindrical shells with a distance of $dr = 1/40\,R$ are generated parallel to the tube axis and the fluid area ratio is determined. A crucial point is to determine the height of the packing. Depending on the packing process the bed can be loosen in the upper part. In the worst case only one sphere can be located on top of the highest layer. Therefore the measured packing height is reduced by one particle diameter to minimize such effects. The local porosity $\varepsilon(r)$ is then calculated by

$$\varepsilon(r) = \frac{A_{fluid}(r)}{A_{cyl}(r)} = \frac{A_{fluid}(r)}{2\pi r h} \tag{1}$$

where A_{fluid} is the fluid shell area, r is the radius of the lateral surface and h the height of the packing. The global porosity ε can be found either by integrating the radial porosity over the tube radius or by determining the ratio of the fluid volume of the bed to a cylinder with the same diameter and height:

$$\varepsilon = \frac{V_{fluid}}{\pi r^2 h}. \tag{2}$$

2.2. Mesh generation

For the mesh generation particle data (diameter and position of the centroid) of the finished DEM simulation are exported. This data is imported into a CAD tool (STAR-Design) and additionally a cylinder with the radius and height of the packing is generated. The resulting CAD geometry is then exported and imported into the CFD program STAR-CCM+ 3.06 for meshing and calculating. Within STAR-CCM+ the first step is a resurfacing of the imported CAD geometry. It can be shown that the used values in Table 2 are a good compromise between accuracy and computational costs.

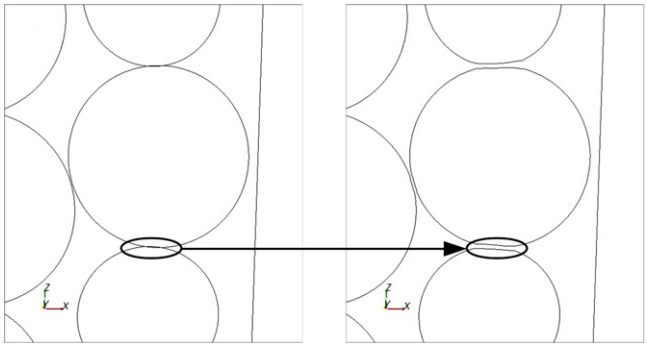

Fig. 1. Modification of the geometry in the near of contact points. Particles are locally flattened if the minimum distance falls below a predefined value.

To avoid the known problems from literature in the near of the particle–particle and particle–wall contact points a new meshing method is used. This method flattens the particles locally in this region as soon as the minimum distance between two surfaces falls below an adequate and predefined value, see Table 2. The flattening is done by moving the vertices of the surface elements which are in close proximity in such a way that a preset minimum distance is kept. The resulting geometry is shown in Fig. 1.

The gap between the particles allows the generation of fluid cells. Due to the fact that the velocity near the contact points is very low the number of cells in the gap can also be kept low and is shown in Fig. 2.

After the resurfacing the existing surface mesh contains a tube wall, one inlet and one outlet and numerous sphere surfaces, which can be handled separately or can be combined and treated as one surface. The next step is to generate a volume mesh made of polyhedrons based on the surface mesh. For the turbulent flow simulation an appropriate resolution of the near wall region is needed. The thickness, the number of extrusion layers and the mesh resolution itself is determined by simulations with varying values for these three parameters and by analyzing the y+-criterion for the boundary layer and the pressure drop over the fixed bed for the mesh resolution. Mesh independency is reached with the values in Table 2.

To minimize the influence of the boundary conditions at the inlet and outlet, the volume mesh is extended by extruding the inlet by

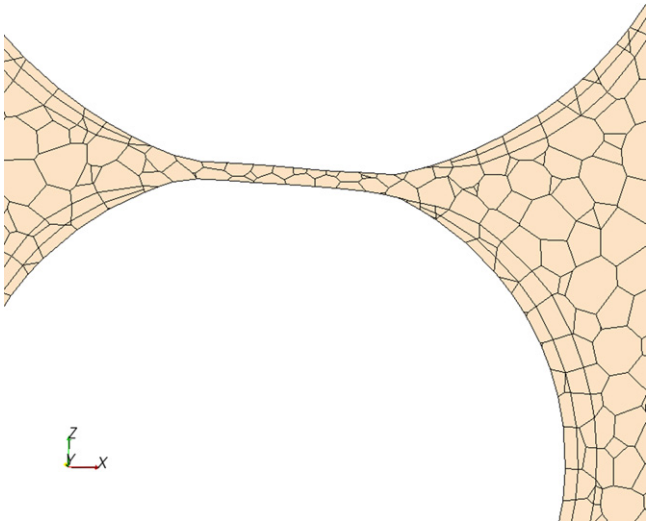

Fig. 2. Fluid cells in the artificial gap between two spheres: a nearly stagnant flow is expected in this region and therefore a low resolution with a maximum of 2 cell layers is sufficient.

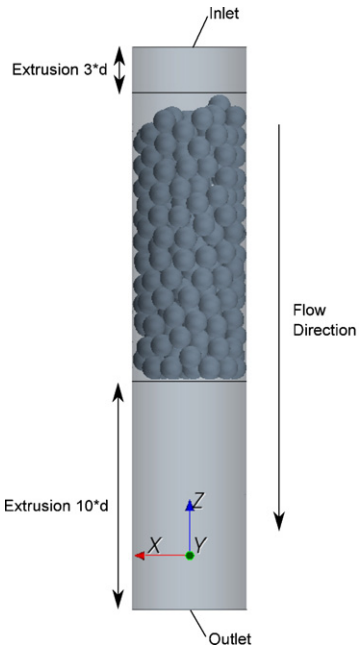

Fig. 3. Schematic reactor overview.

3 and the outlet by 10 particle diameter. Fig. 3 gives a schematic overview.

To estimate the influence of the flattening on the porosity, a sphere with diameter d which is located in the center of a cube with edge length d is meshed with the parameters according to Table 2. The resulting porosity is compared with the analytical result. The total deviation of the porosity is 0.5%. This value includes the deviation caused by the flattening as well as the inevitable deviation caused by the approximation of the surface of the spheres with plane elements.

2.3. CFD setup

For the CFD simulations STAR-CCM+ is used, which is based on the finite volume method. The flow is assumed to be isothermal and incompressible with the physical properties of air ($\eta = 1.577\,e^{-5}\,m^2/s$, $\rho = 1.1767\,kg/m^3$). Tube wall as well as the particle surfaces are defined as 'no-slip' wall and the outlet is defined as 'pressure-outlet' with $p = 1.0$ bar. At the 'velocity'-inlet a constant profile is specified. Each geometry is simulated three times with three different inlet-velocities, which correspond to particle Reynolds numbers

$$Re_P = \frac{v_0 \cdot d}{\eta} \tag{3}$$

of $Re_P = 1$ (laminar), $Re_P = 100$ (transition) und $Re_P = 1000$ (turbulent). If it is needed, turbulence modeling is done with the realizable k–ε model and 'all y+-treatment'.

Pressure drop over the fixed bed is calculated with area-averaged values at the inlet and outlet. The additional pressure drop of the empty tube in front of and behind the fixed bed is several orders of magnitude smaller and can be neglected.

In Table 3 the generated and validated geometries and the corresponding number of cells for the meshes are listed.

For all geometries the whole process consisting of packing generation, meshing and running the simulation with three different Reynolds numbers takes between one and three days depending on the number of fluid cells, which scales with the number of particles. All simulations were done on one processor (Intel Q9550, 2.83 GHz, 8GB RAM). In parallel a significant speed-up can be obtained, which

scales almost linearly with the number of CPUs used as long as the cells per CPU do not fall below a critical value.

It should be noted, that the mesh generation is currently a limiting factor. The bed generation with DEM can easily be extended to thousands of particles even on a desktop PC. CFD calculations with meshes with several 10 million of cells can be run in parallel on clusters. But the automatic mesh generation is very RAM demanding and with the computer stated above (8 GB RAM) a mesh for a maximum of around 800 spheres (or approximately 6 million volume cells) can be generated. One way to overcome this problem is to divide the fixed bed into smaller regions, to mesh each region separately and to combine them in the end. But this is not yet investigated by the authors.

3. Results

3.1. Local porosity

Fig. 4 shows the radial porosity for a couple of D/d ratios. At a wall distance $z = 0$ porosity has its maximum of $\varepsilon = 1$ because the particles contact the confining wall only at a point. With increasing z the porosity becomes smaller and a first minimum can be found at approximately half the sphere diameter. The further run of the curve shows a declining oscillation around the averaged bed porosity.

Table 3
Mesh size, D/d ratio and number of spheres for the generated and validated geometries.

D/d	Number of spheres	Number of cells
3	80	1.0e6
4	50, 100, 130, 200	0.7e6, 1.2e6, 1.5e6, 1.7e6
5	250	2.6e6
6	300	2.8e6
7	400	3.0e6
8	500	4.6e6
10	750	5.7e6

The radial porosity of the generated fixed bed is compared with the empirical equation by de Klerk [16]. de Klerk has derived an equation for the radial porosity as a function of the normalized wall distance by analyzing measurements and data found in literature for different D/d ratios:

$$\begin{aligned} \varepsilon(r) &= 2.14z^2 - 2.53z + 1 && \text{if } z \le 0.637 \\ \varepsilon(r) &= \varepsilon_b + 0.29\exp(-0.6z)\cdot[\cos(2.3\pi(z-0.16))] \\ &\quad + 0.15\exp(-0.9z) && \text{if } z > 0.637 \end{aligned} \tag{4}$$

with the normalized wall distance $z = (R - r)/d$ and ε_b the bed porosity far away from the wall.

This equation reflects literature data with a relative error of maximum 20% with an increase in difference with smaller D/d values. The first part of this equation describes a quadratic decline in the near wall region whereas the second part describes the radial porosity with a sinusoidal declining function.

Fig. 4 shows that the radial porosity distribution extracted from DEM simulations matches the correlation by de Klerk [16] quite well. Amplitude as well as frequency of the declining oscillation can be reproduced. The maximum deviation is mainly found near the axis of the tube. Remarkable is the increase in porosity at $z = 2$ for a D/d ratio = 4. Contrary to the prediction of Eq. (4) a channel is formed in the middle of the tube (Fig. 5). Such a channel is formed regardless of the manner of the bed generation and is a result of the structuring effect of the confining walls in combination with a high friction coefficient, which prevents a sliding of the particles towards the middle axis. This behaviour was found experimentally by Kritschke [17]. On the other hand, Eq. (4) is not capable to describe such an effect because of its structure.

3.2. Global porosity

The global bed porosity influences significantly the pressure drop calculation of fixed beds. Therefore an accurate prediction of this value is important. In Fig. 5 the porosity of the generated fixed

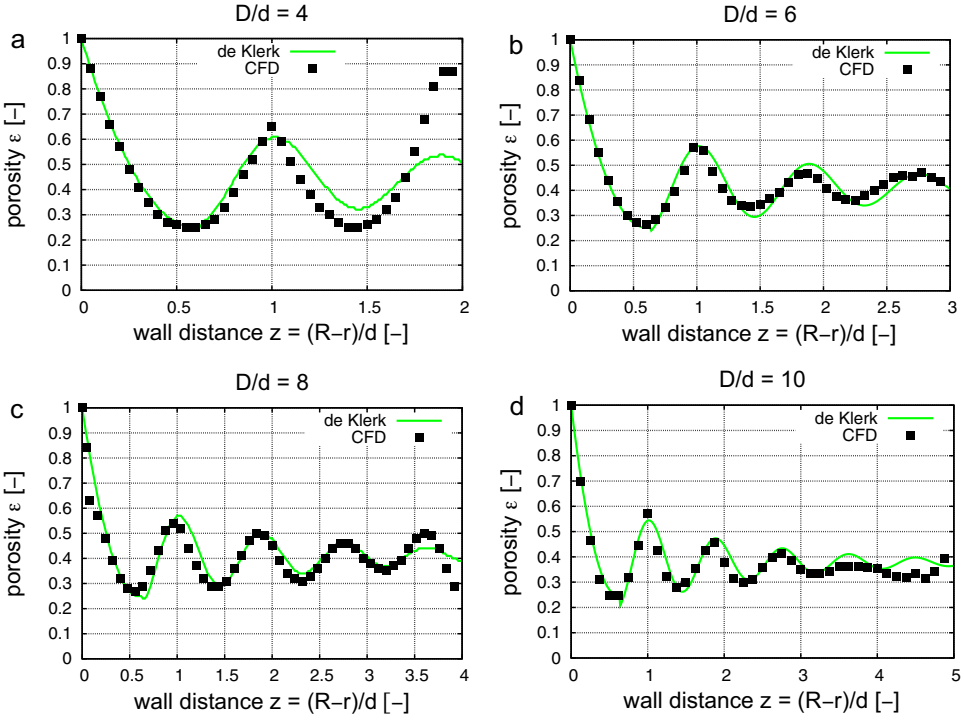

Fig. 4. Radial porosity distribution for different D/d ratios: (a) $D/d = 4$, (b) $D/d = 6$, (c) $D/d = 8$ and (d) $D/d = 10$.

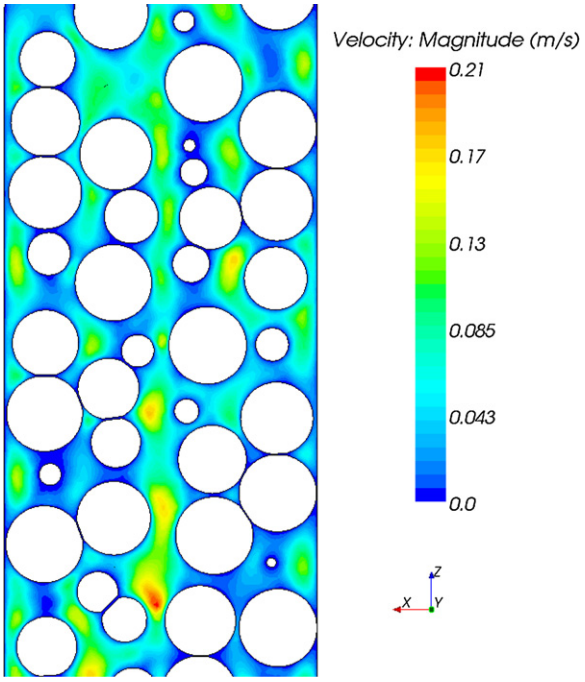

Fig. 5. Generated channel in the middle of the tube at $D/d = 4$.

beds are compared with the empirical correlation by Dixon [13]:

$$\varepsilon = 0.4 + 0.05\left(\frac{d}{D}\right) + 0.412\left(\frac{d}{D}\right)^2 \tag{5}$$

Dixon has modified an empirical formula by Aerov [14] to match the analytical void fraction calculated by Carman [15]. The global bed porosity becomes $\varepsilon = 0.4$ when the D/d ratio goes to infinity. On the other hand the porosity increases for smaller D/d values. This is caused by an increasing influence of the confining wall.

The values extracted from the simulations match the empirical values. The maximum deviation in the investigated D/d range is 2.4% (Fig. 6).

3.3. Pressure drop

To validate the calculated pressure drop Eq. (6) by Eisfeld and Schnitzlein [18] is used. Eisfeld and Schnitzlein have adapted the parameters for the friction coefficient of Reichelt's correlation [19] by analyzing several thousand data points. The pressure drop is

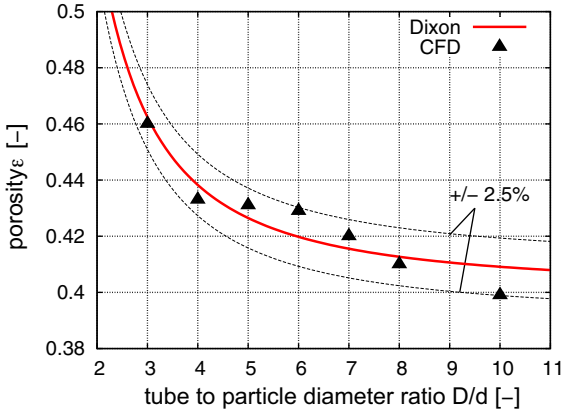

Fig. 6. Global fixed bed porosity for different D/d ratios.

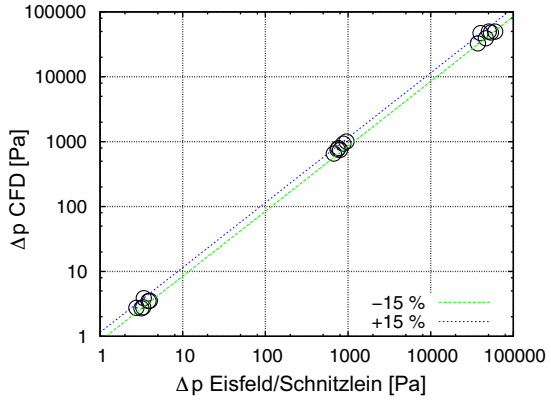

Fig. 7. Pressure drop over the fixed bed: the data cloud on the left-hand side represents different D/d ratios at $Re_P = 1$, the central one at $Re_P = 100$ und the right-hand side at $Re_P = 1000$.

defined by

$$\Delta p = \left(154 \cdot A_w^2 \cdot \frac{(1-\varepsilon)^2}{\varepsilon^3} \cdot \frac{1}{Re_P} + \frac{A_w}{B_w} \cdot \frac{(1-\varepsilon)}{\varepsilon^3}\right) \cdot \frac{L}{d} \cdot \rho \cdot v_0^2 \tag{6}$$

with the coefficients A_w and B_w

$$A_W = 1 + \frac{2}{3 \cdot D/d} \cdot (1-\varepsilon) \tag{7}$$

$$B_W = \left[1.15 \cdot \left(\frac{d}{D}\right)^2 + 0.87\right]^2 \tag{8}$$

which consider the influence of the D/d ratio and therefore the influence of the confining walls. The parity plot in Fig. 7 shows good agreement between the CFD calculations and Eq. (6) in all flow regimes as well as for all investigated D/d ratios. The maximum deviation is 15% and is found once in the laminar and once in turbulent flow regime.

3.4. Velocity distribution

An important characteristic for the flow through a fixed bed is its velocity distribution. A general overview is shown in Fig. 8 where the local velocity component in axial direction normalized with the inlet velocity is displayed. Locally an increase up to a factor of 11 is found in areas where the packing is not so dense. Regions with stagnant or backflow appears in the wake of the particles and at the end of the fixed bed.

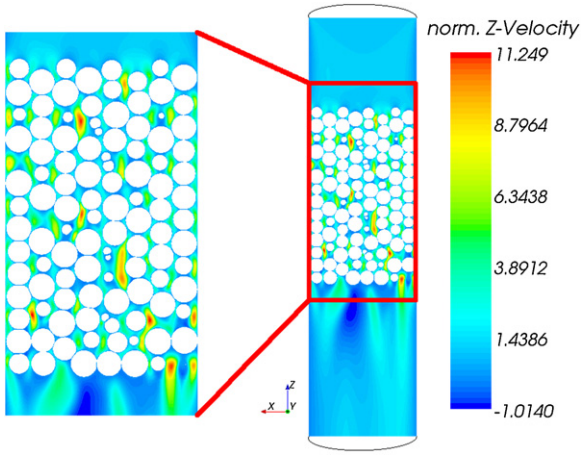

Fig. 8. Axial velocity normalized with the inlet velocity for $Re_P = 100$ and $D/d = 7$.

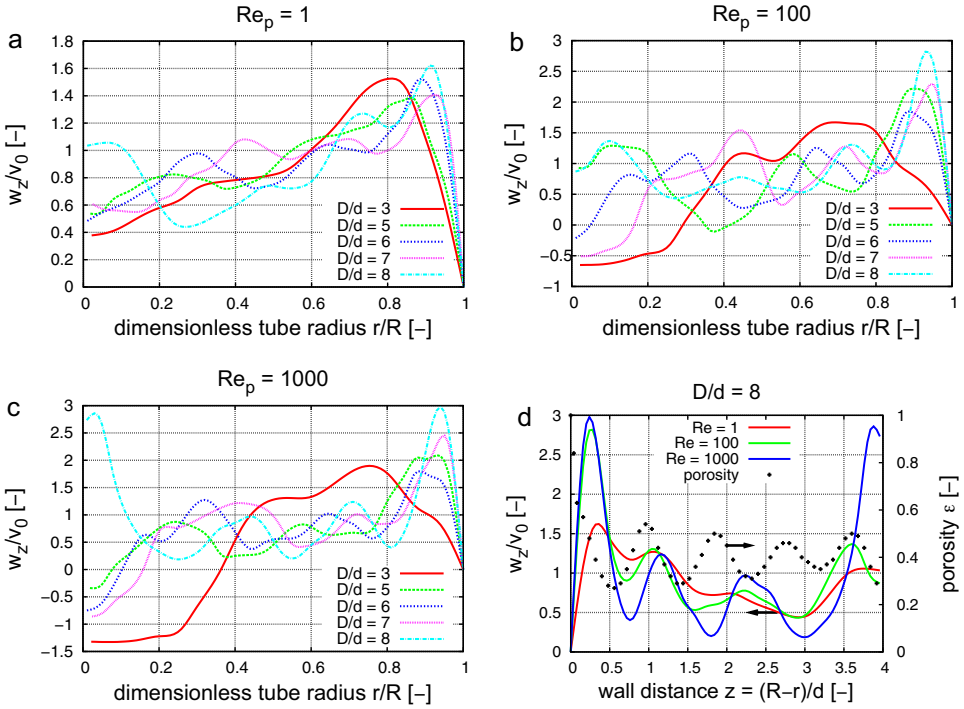

Fig. 9. Circumferential-averaged axial velocity profile at a cross-section behind the end of the fixed bed for (a) $Re_P = 1$, (b) $Re_P = 100$ and (c) $Re_P = 1000$ and different D/d ratios. Figure (d) compares the velocity distribution for $D/d = 8$ and different Re_P with the radial porosity distribution.

In Fig. 9a–c the circumferential-averaged axial velocity over the tube radius in a cross-section at the end of the fixed bed is shown. For all Re_P-numbers and for all D/d ratios the highest velocities are found in the near-wall region, where the porosity has its highest values. Remarkable is the high velocity for $Re_P = 1000$ and a D/d-ratio = 8 near the middle-axis ($r/R \sim 0.25$): this is caused by a channel which is formed in the last particles layers. This verifies the arguments by Drahos et al. [6].

Furthermore regions with stagnant or backflow occur only for $Re_P \geq 100$ although these regions also exist for $Re_P = 1$ within the bed. For laminar flow, these regions are very small, around 1% of the whole fluid volume in the packed bed. On the cross-section after the bed no areas with backflow can be detected. For the transitional and turbulent flow regime the volume of these regions increases up to a volume fraction of 11% and 12.5%, respectively and can be detected on the cross-section behind the bed.

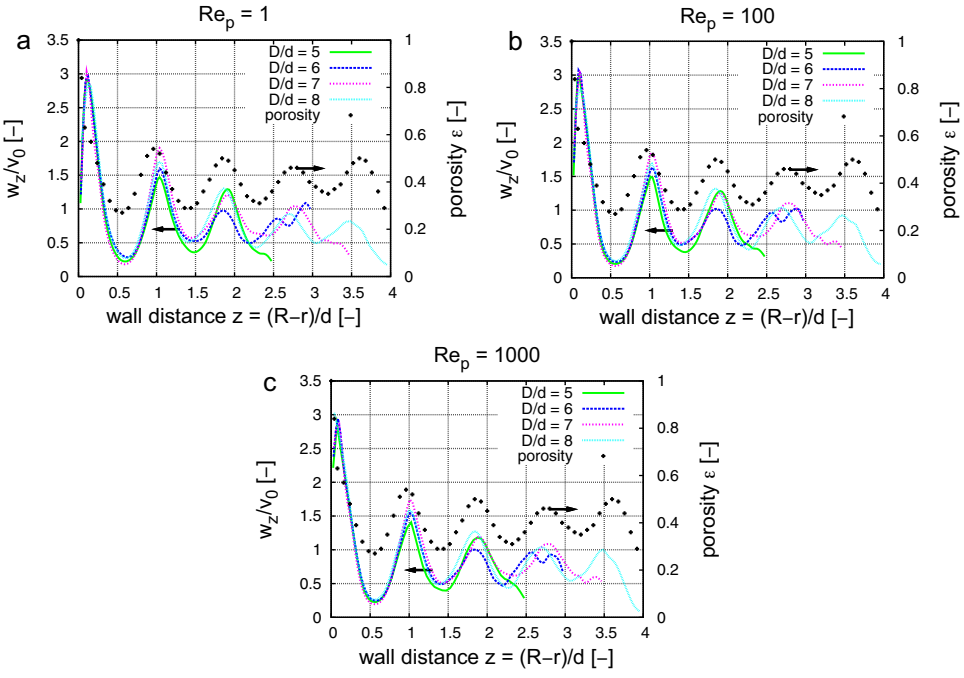

Fig. 10. Circumferential-averaged axial velocity profile calculated from velocity values within the bed for (a) $Re_P = 1$, (b) $Re_P = 100$ and (c) $Re_P = 1000$ and different D/d ratios.

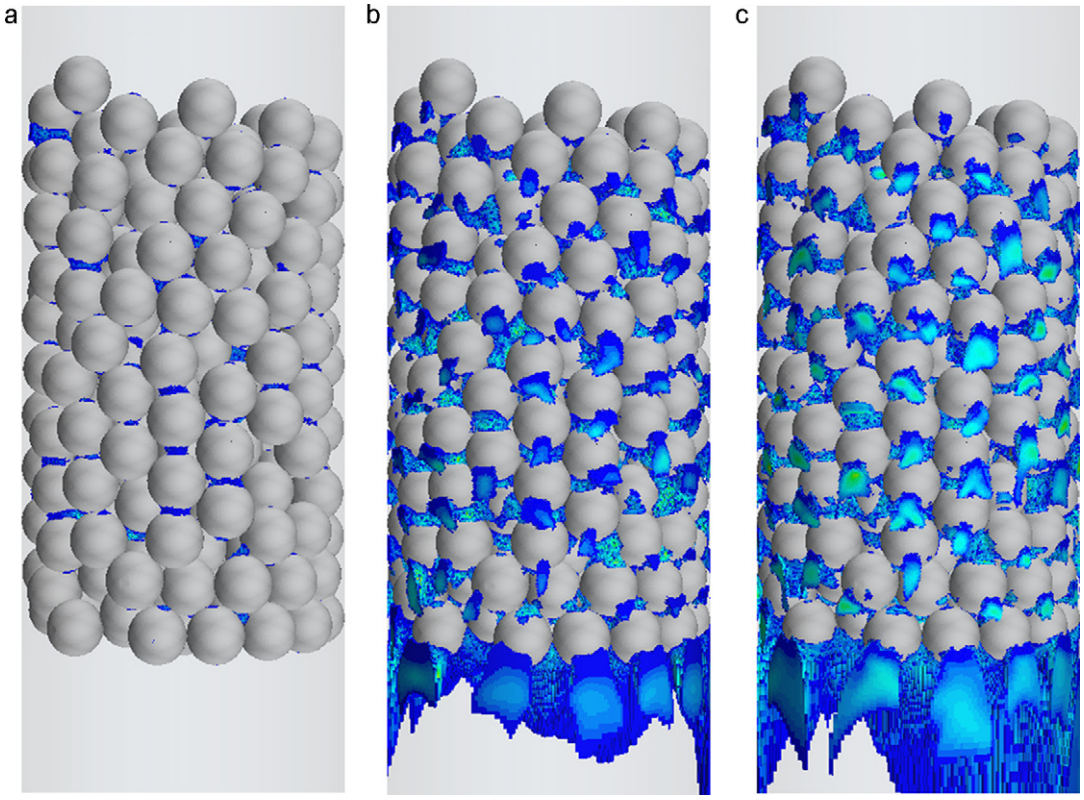

Fig. 11. Regions with zero or negative velocities for (a) $Re_P = 1$, (b) $Re_P = 100$ and (c) $Re_P = 1000$.

In Fig. 9d, the radial porosity distribution and the circumferential-averaged axial velocity for a D/d ratio = 8 is plotted. A clear correlation between the velocity distribution and the radial bed porosity cannot be identified.

A second method to evaluate the velocity distribution inside the bed was used: the velocities in the bed were volume averaged in radial direction. These interstitial velocities are then multiplied by the local porosity to obtain the artificial velocity (Freund [20]). These velocities are displayed in Fig. 10a–c. Similar to the obtained results from the cross-section behind the packing, the highest velocities were found next to the wall. The w_z/v_0 velocity ratio is in the range of 2.5–3 which corresponds to values found by Giese et al. [5] and Freund [20]. The oscillations of the radial flow profiles reflect the oscillations of the radial porosity distribution.

It should be noted, that for all Re_P the velocity values are always positive. This means that the regions with stagnant and backflow inside the packing get lost during averaging. In Fig. 11a–c all volume cells with zero or negative velocity are displayed. The volume fraction of this region increases with increasing Re-number and reaches a value of around 13%. This influences the residence time distribution: the residence time is short in the near wall region, while the residence time in the regions with stagnant or back flow is high.

4. Conclusion

In this work a new method for meshing spherical fixed beds is presented. The method is capable to predict the local and global porosity as well as the pressure drop accurately. During the mesh generation the particles are flattened automatically near the particle–particle and particle–wall contact points. In contrast to known methods, the modification of the geometry is small and subsequent corrections of the porosity or pressure drop is not needed.

Furthermore, the whole process consisting of the random fixed bed generation with DEM, CAD model generation, meshing and running the CFD simulation is fully automated and results can be obtained within hours.

Likewise this method can be adopted easily on any kind of particle shape like cylinders or more general on any kind of contact point problem.

The modeling approach for a radial varying velocity is a significant improvement compared to the plug flow assumption. Nevertheless this model cannot account for regions with stagnant or back flow. The influence of such regions has to be investigated.

Thus a spatially resolved CFD simulation of fixed bed reactors with a small D/d ratio is helpful and reasonable for a better understanding of, e.g. lab-scale reactors for heterogeneous catalysis. For such reactors it is important to know the concentration and temperature fields exactly and, at the moment, only by using CFD this knowledge can be obtained in short time.

Acknowledgements

This work is part of the Cluster of Excellence “Unifying Concepts in Catalysis” coordinated by the Technische Universität Berlin. Financial support by the Deutsche Forschungsgemeinschaft (DFG) within the framework of the German Initiative for Excellence is gratefully acknowledged (EXC 314).

References

[1] O. Kalthoff, D. Vortmeyer, Ignition/extinction phenomena in a wall cooled fixed-bed reactor—experiments and model-calculations including radial porosity and velocity distributions, Chem. Eng. Sci. 35 (1980) 1637–1643.
[2] D. Vortmeyer, R.P. Winter, On the validity limits of packed-bed reactor continuum models with respect to tube to particle diameter ratio, Chem. Eng. Sci. 39 (1984) 1430–1432.
[3] T. Daszkowski, G. Eigenberger, A reevaluation of fluid-flow, heat-transfer and chemical-reaction in catalyst filled tubes, Chem. Eng. Sci. 47 (1992) 2245–2250.

[4] O. Bey, G. Eigenberger, Fluid flow through catalyst filled tubes, Chem. Eng. Sci. 52 (1997) 1356–1376.
[5] M. Giese, K. Rottschäfer, D. Vortmeyer, Measured and modeled superficial flow profiles in packed beds with liquid flow, AIChE Journal 44 (1998) 484–490.
[6] J. Drahos, J. Cermak, I. Ziolkowska, D. Ziolkowski, Statistical analysis of local gas velocities an the exit from a packed bed, Chem. Eng. Sci. 24 (1982).
[7] P.A. Cundall, O.D.L. Strack, A discrete numerical model for granular assemblies, Géotechnique 29 (1979) 47–65.
[8] H. Bai, J. Theuerkauf, P.A. Gillis, P.M. Witt, A coupled DEM and CFD simulation of flow field and pressure drop in fixed bed reactor with randomly packed catalyst particles, Ind. Eng. Chem. Res. 48 (2009) 4060–4074.
[9] T. Atmakidis, E.Y. Kenig, CFD-based analysis of the wall effect on the pressure drop in packed beds with moderate tube/particle diameter ratios in the laminar flow regime, Chem. Eng. J. 155 (2009) 404–410.
[10] A. Guardo, M. Coussirat, M. Angels Larrayoz, F. Recasens, E. Egusquiza, CFD flow and heat transfer in nonregular packings for fixed bed equipment design, Ind. Eng. Chem. Res. 43 (2004) 7049–7056.
[11] S. Ookawara, M. Kuroki, D. Street, K. Ogawa, High-fidelity DEM-CFD modeling of packed bed reactors for process intensification, in: Proceedings of European Congress of Chemical Engineering (ECCE-6), Copenhagen, 16–20 September, 2007.
[12] M. Leva, M. Grummer, Pressure drop through packed tubes, Part III: Prediciton of voids in packed tubes, Chem. Eng. Prog. 43 (1947) 713–718.
[13] A. Dixon, Correlations for wall and particle shape effects on fixed bed bulk voidage, Can. J. Chem. Eng. 66 (1988) 705–708.
[14] M.E. Aerov, Some Problems on Aerodynamics and Heat Exchange in Catalytic Reaction Vessels, PhD Thesis, Moscow (1951).
[15] P.C. Carman, Fluid flow through granular beds, Trans. Inst. Chem. Eng. 15 (1937) 150–166.
[16] A. de Klerk, Voidage variation in packed beds at small column to particle diameter ratio, AIChE J. 49 (2003) 2022–2029.
[17] A. Kritschke, Modellierung und experimentelle Untersuchung von Transportprozessen in durchströmten Schüttungen, PhD Thesis, München (2001).
[18] B. Eisfeld, K. Schnitzlein, The influence of confining walls on the pressure drop in packed beds, Chem. Eng. Sci. 56 (2001) 4321–4329.
[19] W. Reichelt, Zur Berechnung des Druckverlustes einphasig durchströmter Kugel- und Zylinderschüttungen, Chem. Ing. Tech. 44 (1972) 1068–1071.
[20] H. Freund, Ortsaufgelöste Simulation von Transportprozessen in durchströmten Festbetten, PhD Thesis, Erlangen (2007).